JOURNAL OF MATERIALS SCIENCE 26 (1991) 2431–2435

Scanning electron microscopy and electron microprobe analysis of Au–GeO_x–Cu and Au–AlO_x–Cu sandwich structures

M. M. EL-SAMANOUDY
Physics Department, Faculty of Education, Ain-Shams University, Cairo, Egypt
J. BEYNON
Department of Physics, Brunel University, Uxbridge, Middlesex UB8 3PH, UK

Direct observations of the counter-electrode surface of electroformed Au–I–Cu sandwich structures (where I is reactively evaporated AlO_x or GeO_x) were carried out using scanning electron microscopy. Electron microprobe analyses of surface defects in electroformed samples, after etching the copper counter-electrode, tended to confirm the presence of copper. Surface defects are identified as the terminations of filament bundles, which supports the filamentary model of conduction.

1. Introduction

Thin-film MIM structures have been shown to exhibit a variety of interesting phenomena subsequent to electroforming [1, 2]. It has been conclusively demonstrated that electroformed MIM sandwich structures (i) undergo a substantial increase in d.c. electrical conductivity by several orders of magnitude, (ii) possess a voltage-controlled (or current-controlled) negative resistance region (VCNR or CCNR), (iii) exhibit memory or switching phenomena, or both, and are electron-emissive and electroluminescent.

Various explanations have been put forward to explain the origin of electroforming in, and the properties of, electroformed MIM devices. The filamentary description of conduction by Dearnaley *et al.* [3] seems to have had the most success, although it has been modified and extended by other workers [4–7]. A comprehensive review of the factors affecting electroforming in MIM structures has been described [8]. More recently, a potential-modified defocusing phase-contrast technique has been used to support the filament-rupturing process [9]. Negative resistance and switching (N- and S-types) have been observed in Al–Al_2O_3–Ag and Ag–GeO–Al structures [10]. Nepjko *et al.* [11] induced switching from the high-conducting to the low-conducting state using the electron beam of a scanning electron microscope.

Following an investigation of threshold-, pressure- and thermal-memory in Al–AlO_x–Cu and Al–GeO_x–Cu sandwich structures [12], the present study concentrates on the origin of counter-electrode damage, and the role in it, if any, of the filament model of conduction.

2. Experimental procedure

The AlO_x and GeO_x insulating films used in the Au–I–Cu sandwich structures were deposited through mechanical masks on to clean Corning 7059 substrates at an average rate of 0.5 nm s^{-1}. The oxides were prepared by the reactive-evaporation of Al and Ge, respectively, in various partial pressures of oxygen (from about 10–100 mPa). The Cu counter-electrode was positively biased throughout the investigations. Film thickness was monitored with a quartz crystal oscillator, but accurate determinations were made via optical interferometry.

After fabrication, the MIM structures were transferred to a scanning electron microscope having a dispersive X-ray detection system and a degree of vacuum $\simeq$ 1 mPa. The highest magnification available was $\times$ 20 000. The accelerating potential difference was usually maintained at 10 kV in order to minimize sample charging.

Electroforming was carried out inside the microscope, and the d.c. I–V characteristics obtained. Visual observations of local phenomena on the counter-electrode of the structures were made at potential differences (PD) below and above V_P, the PD corresponding to the peak current in the d.c. I–V characteristic. No clear observations of the electrode were possible at V_P.

Argon ion-beam etching of the counter-electrode and dielectric was employed, together with electron microprobe analysis, in an attempt to confirm the presence of metallic filaments. The angle of incidence of the argon ions used for etching lay between 25° and 65°, relative to the surface of the film. The counter-electrode was etched-off completely for the electron microprobe analysis study, and the exposed dielectric was carbon-coated to prevent surface charging. The microscope's dispersive X-ray detection system enabled the spatial distribution of Ge, Al and Cu to be determined.

0022–2461/91 $03.00 + .12

3. Results and discussion

3.1. Electroforming and *I–V* characteristics

Fig. 1 shows a typical d.c. *I–V* characteristic for an electroformed Au–AlO_x–Cu structure, 60 nm thick; the AlO_x film was prepared at an oxygen partial pressure of 100 mPa. Electroforming was initiated at a threshold PD of about 2.5 V with AlO_x and 8 V with GeO_x. Maintaining the PD constant above these values resulted in the conductivity increasing rapidly with time.

The electroforming process can be interpreted on the basis of the filamentary conduction model [3]. Filaments probably arise as a result of the injection of positively charged copper ions from the counter-electrode: the filaments are non-uniform in cross-section, possessing weak regions, which become heated due to electron flow. Thus, there is the possibility that electron–phonon scattering may occur at weak hot spots, leading to eventual rupture of the filament. Using Fig. 1, the peak power level may be calculated to be 0.35 W, which is high enough for a significant amount of joule heating to occur, with consequent filament rupture and the presence of a negative resistance region.

3.2. Scanning electron microscopy: sample damage

Prior to the onset of electroforming, no special features were observed on the counter-electrode; the electron beam was moved over the electrode surface to search for local structural changes at each setting of the sample PD. Fig. 2 for AlO_x and Fig. 3 for GeO_x show that the counter-electrode surface has been severely damaged during the electroforming process. A large number of tiny holes of various sizes can be observed – the bright spots are believed to be sites of high electron emission. Further surface damage occurred on increasing the PD above threshold. Such damage may have been caused by a series of events: thermal-runaway in filaments located in that region; the production of gas bubbles; gas emission; surface peeling/melting. Fig. 4a and b were obtained with a 50 nm thick Cu counter-electrode after biasing at + 7 V for AlO_x and + 10 V for GeO_x, respectively. The bubble of gas in Fig. 4c (most probably oxygen generated in an electrolytic process [6]) is about 10 μm in diameter. Fig. 5a shows a destructive event that occurred at + 15 V and exposed the underlying dielectric. The average diameter of the damaged region is 6 μm. Fig. 5b depicts the general surface appearance at the lower magnification of × 1000. Tree-branch defects, originating at high electric field regions, are observable.

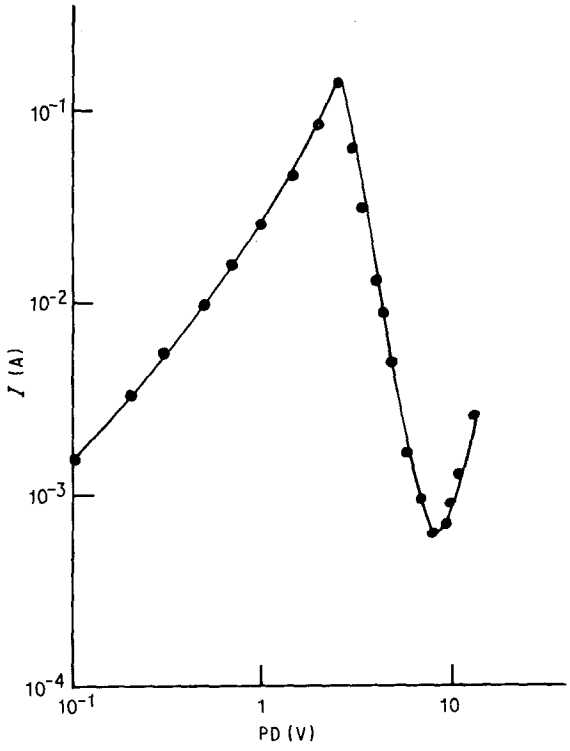

Figure 1 D.c. *I–V* characteristics for an electroformed Au–AlO_x–Cu sandwich structure at 20 °C.

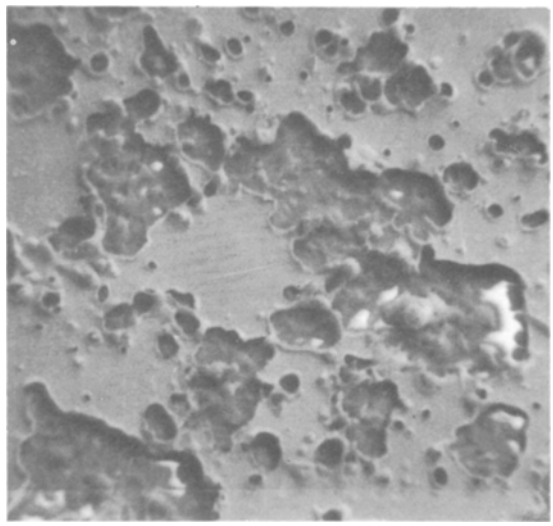

Figure 2 Scanning electron micrograph showing counter-electrode damage to an Au–AlO_x–Cu structure; O_2 partial pressure ≃ 10 mPa, (× 2000).

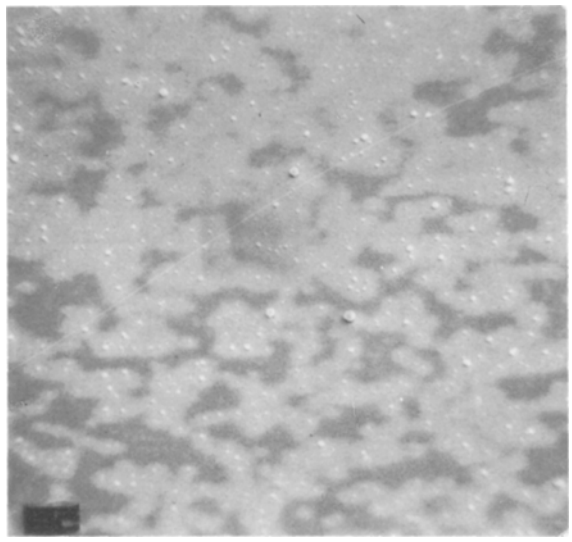

Figure 3 Scanning electron micrograph showing counter-electrode appearance of an Au–GeO_x–Cu structure; O_2 partial pressure ≃ 8 mPa, (× 1000).

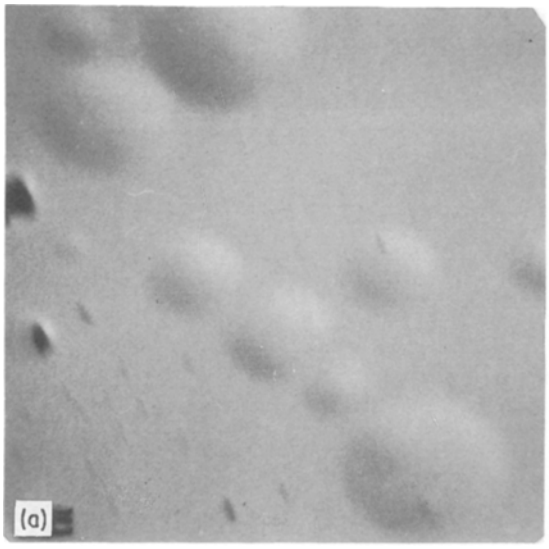

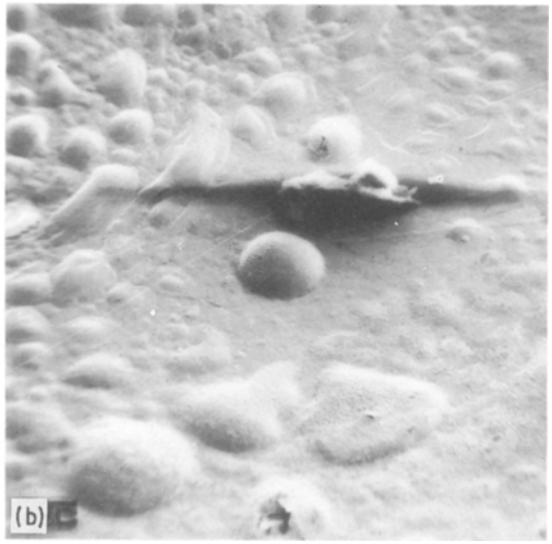

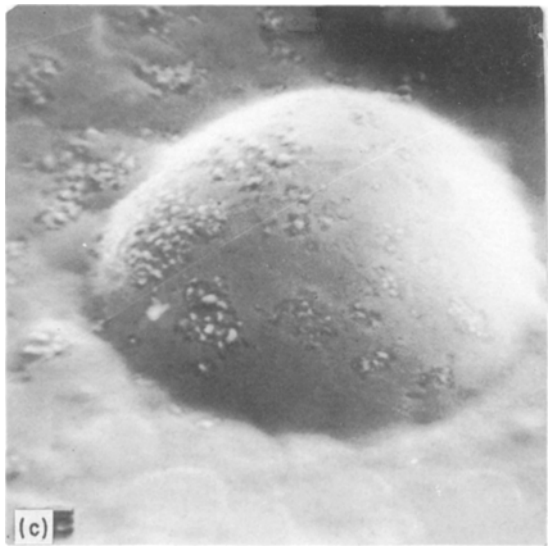

Figure 4 (a) Gas bubbles at the surface of the Cu counter-electrode after biasing an Au–AlO_x–Cu structure at 7 V; AlO_x thickness is 60 nm, (× 1000). (b) Gas bubbles formed after biasing an Au–GeO_x–Cu structure at 10 V, (× 1000). (c) Gas bubble at the centre of the active area in (b) (× 5000).

3.3. Filament observations and electron microprobe analysis

In this study two samples were prepared on the same substrate. One sample was in the ON-state, whereas the other, a control sample, had not been electroformed. The control was used for comparison purposes only. Fig. 6 is a scanning electron micrograph of the central area of a defect on an Au–GeO_x–Cu sample after etching the counter-electrode and 10 nm of the dielectric; the GeO_x was prepared at 26 mPa. Cu and Ge scan lines obtained from the microprobe analysis are superimposed on the defect. The centre of the defect has an excess of Cu, which may be interpreted as the termination of a bundle of filaments. No significant variation in Ge or Cu was observed for the control sample, so that within the limit of detection of the equipment the dielectric appears to have preserved its initial structure.

Clearer examples of possible filament terminations in an electroformed Al–AlO_x–Cu sample are shown in Fig. 7a and b. These figures indicate that the edges of the defects have an excess of Cu, which must have diffused into the dielectric from the counter-electrode, whereas in the central regions of the defects the Al

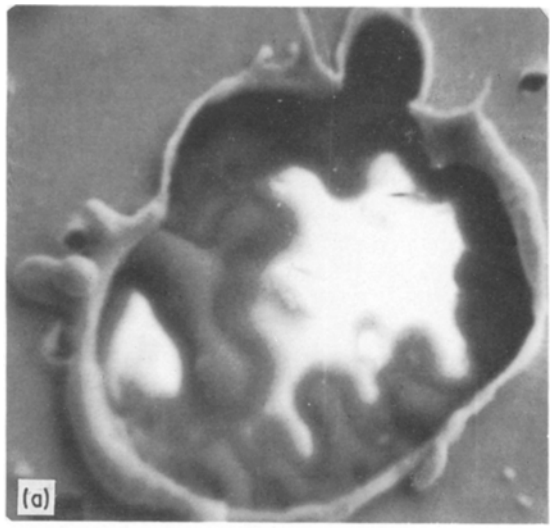

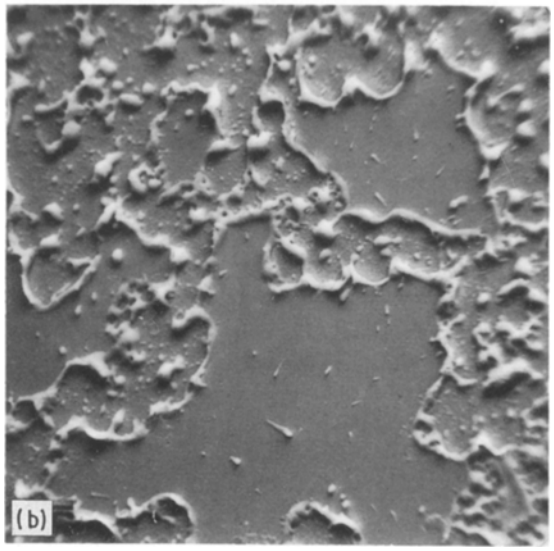

Figure 5 (a) Destructive surface damage of an Au–AlO_x–Cu structure held at 15 V, (× 10000). (b) Tree-branch defects (× 1000).

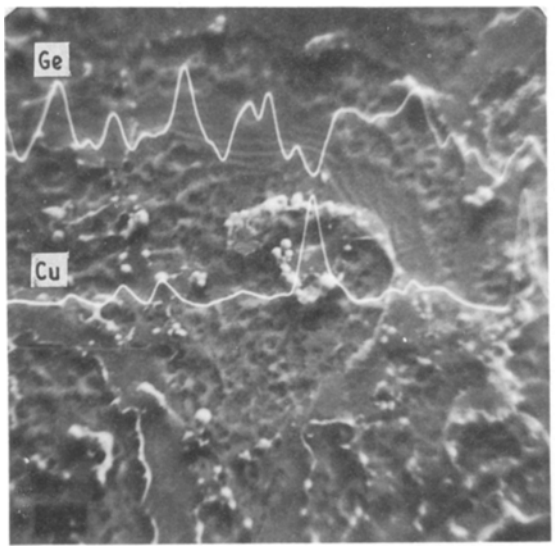

Figure 6 Scanning electron micrograph with superimposed electron-microprobe traces for an Au–GeO_x–Cu structure (× 1000).

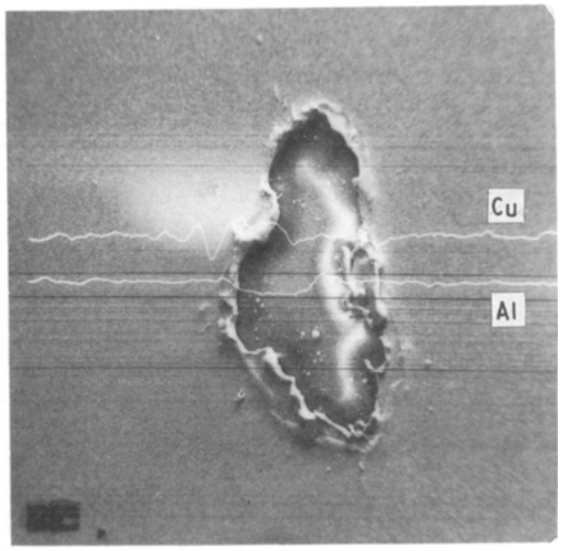

Figure 8 Scanning electron micrograph and micro-probe traces of a sample electroformed outside the microscope, (× 1000).

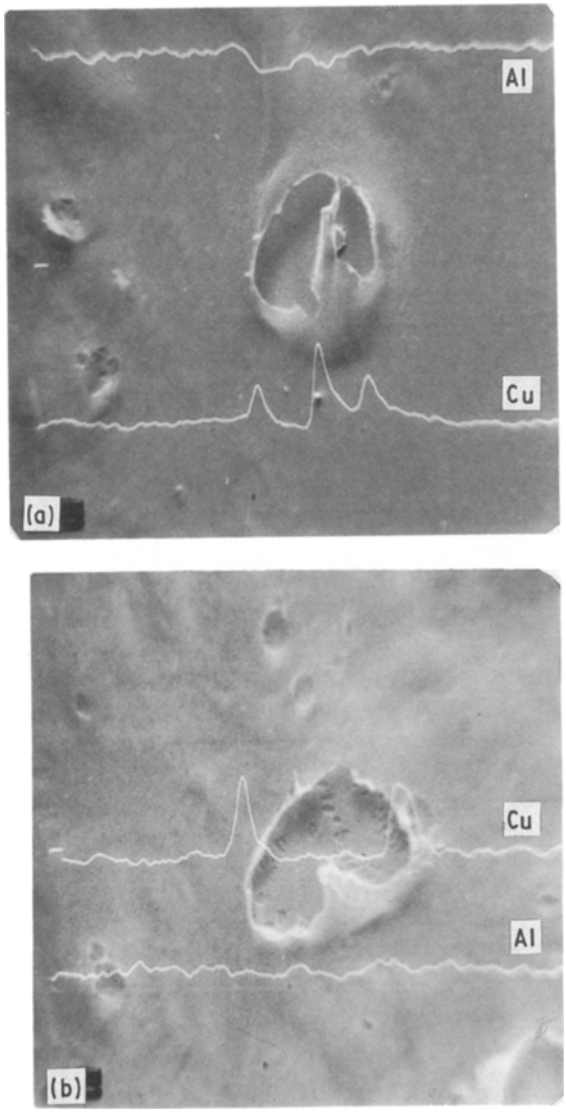

Figure 7 (a),(b) Electron-microprobe traces and defects in etched Al–AlO_x–Cu structures; O_2 partial pressure: 80 mPa; AlO_x thickness: 50 nm, (× 2000).

concentration is almost constant. Therefore, conduction predominantly occurs through the Cu-rich region.

The inference that such local surface features are the terminations of filament bundles rests on the fact that during the cooling phase, e.g. after a switching event, a separation of dielectric and filamentary material occurs owing to differences in their freezing points. A new microcrystalline phase can be formed if the rate of cooling is sufficiently high. This conclusion also suggests that the remainder of the dielectric matrix does not play any major role in the switching process and thereby retains its amorphicity. These results are in broad agreement with those of Park and Basavaiah [13] who studied Zr–ZrO_2–Au. They also found that physical changes occurred to the counter-electrode during electroforming and in switching from OFF-state to ON-state. Sie *et al.* [14] observed the generation of crystalline filaments in active films of $Cr_{15}Te_{81}X_4$, where X is an additive designed to improve device memory and lifetime, using a set-pulse of 10 ms duration and 4 mA amplitude; the filaments disappeared on applying a reset-pulse. Fig. 8 is a scanning electron micrograph of a sample electroformed outside the microscope, and which had been switched a number of times in a memory-behaviour investigation. It is clear that there is a build-up of Cu near the one edge of the defect. The white Cu-deficient region is produced by specimen-charging by the electron beam; evaporation of diffused Cu under local heating by the electron beam may explain the absence of Cu peaks in the scan lines. These results are in agreement with those of Manhart [15, 16], Al-Ismal and Hogarth [17] and Morgan and Howes [18] with pure SiO films, and Al-Ramadhan and Hogarth [19] with SiO/V_2O_5 mixed oxide films. Therefore, it may be concluded that metallic diffusion of electrode material appears to be an essential pre-requisite for switching to the low-resistance ON-state in AlO_x and GeO_x dielectric films.

Acknowledgements

One of us (MM El-S) thanks Professor A. A. El-Shazly, Ain-Shams University for his encouraging

contributions and stimulating discussions. Our thanks, also, to Mr R. Bulpett, Experimental Techniques Centre, Brunel University, for experimental assistance with the scanning and microprobe investigations, and helpful discussions.

References

1. T. W. HICKMOTT, *J. Appl. Phys.* **36** (1965) 1885.
2. R. R. VERDERBER and J. G. SIMMONS, *Radio Electron. Engng* **33** (1967) 347.
3. G. DEARNALEY, D. V. MORGAN and A. M. STONEHAM, *J. Non-Cryst. Solids* **4** (1970) 593.
4. R. R. SUTHERLAND, *J. Phys. D* **4** (1971) 468.
5. J. E. RALPH and J. M. WOODCOCK, *J. Non-Cryst. Solids* **7** (1972) 236.
6. A. E. RAKHSHANI, C. A. HOGARTH and A. A. ABIDI, *ibid.* **20** (1976) 25.
7. J. LI and J. BEYNON, *Phys. Status Solidi.* Forthcoming.
8. A. K. RAY and C. A. HOGARTH, *Int. J. Elect.* **57** (1984) 1.
9. H. PAGNIA, K. SCHLEMPER and N. SOTNIK, *Mater. Lett.* **5** (1987) 260.
10. SH. M. ALEKPEROVA, V. A. VETKHOV, G. S. GADZHIEVA, F. D. KASINOV and V. M. MAMIKONOVA, *Telecommun. Radio Engng Part 2* **41** (1986) 89.
11. S. A. NEPJKO, H. PAGNIA and V. I. STYOPKIN, *Phys. Status Solidi (a)* **90** (1985) K113.
12. J. BEYNON and M. M. EL-SAMANOUNDY, *J. Mater. Sci. Lett.* **6** (1987) 1447.
13. K. C. PARK and S. BASAVAIAH, *J. Non-Cryst. Solids.* **2** (1970) 284.
14. C. H. SIE, M. P. DUGAN and S. C. MOSS, *ibid.* **8–10** (1972) 877.
15. S. MANHART, *J. Phys. D* **6** (1973) 82.
16. *Idem., J. Non-Cryst. Solids.* **11** (1973) 293.
17. S. A. AL-ISMAL and C. A. HOGARTH, *J. Mater. Sci.* **20** (1985) 2186.
18. D. V. MORGAN and M. J. HOWES, *Thin Solid Films* **20** (1974) S7.
19. F. A. S. AL-RAMADHAN and C. A. HOGARTH, *J. Mater. Sci.* **19** (1984) 1939.

Received 5 July
and accepted 1 August 1990